Available online at www.sciencedirect.com
SCIENCE DIRECT®
European Journal of Pharmaceutics and Biopharmaceutics 58 (2004) 301–316
European Journal of Pharmaceutics and Biopharmaceutics
www.elsevier.com/locate/ejpb

Review article

Visualization of skin penetration using confocal laser scanning microscopy

R. Alvarez-Román[a,b,c], A. Naik[a,c], Y.N. Kalia[a,c], H. Fessi[a,b], R.H. Guy[a,c,*]

[a]*Centre interuniversitaire de recherche et d'enseignement, Universities of Geneva and Lyon, Archamps, France*
[b]*UMR CNRS 5007, Claude Bernard University, Lyon, France*
[c]*School of Pharmacy, University of Geneva, Geneva, Switzerland*

Received 24 October 2003; accepted in revised form 22 March 2004

Available online 1 June 2004

Abstract

The use of skin as an alternative route for administering systemically active drugs has attracted considerable interest in recent years. However, the skin provides an excellent barrier, which limits the number of drug molecules suitable for transdermal delivery. Thus, in order to improve cutaneous delivery, it is necessary to adopt an enhancement method, either (i) passively using novel formulations, e.g. microemulsions, liposomes, and colloidal polymeric suspensions, or more conventional skin permeation enhancers, or (ii) with a physical approach, such as, iontophoresis, sonophoresis or electroporation. Although there has been much progress, the precise modes of action of the different techniques used are far from well-understood. The objective of this review, therefore, is to evaluate how confocal laser scanning microscopy may contribute to the determination of the mechanisms of diverse skin penetration enhancement strategies.

Keywords: Confocal laser scanning microscopy; Skin; Fluorescent visualization; Fluorescent probes

1. Introduction

Light and electron microscopy have been important tools for the analysis of cellular structure, physiology and function of biological tissues. Although transmission electron microscopy (TEM), offers excellent resolution of ultrastructural details (~0.1 nm) for skin visualization, it causes damage to the specimen and suffers from fixation and sectioning artefacts. Only small specimen areas can be directly visualized and quantification of a permeating drug molecule is impossible [1,2]. In addition, TEM provides static two-dimensional images that are difficult to reconstruct three-dimensionally from serial sections [3].

Conventional light microscopy allows direct examination of viable as well as fixed cells and tissues and dynamic processes can be therefore observed and analysed quantitatively. However, ultrastructural details cannot be obtained because of the relatively low resolution (0.2 μm); moreover, the specimen requires fixation and sectioning, which can lead to artefacts. Localization of a permeating molecule is possible, for example, with a fluorescent [2,4] or radioactive tracer [5], but out-of-focus information can undermine the quality and clarity of the images, especially in thick specimens with overlapping structures. Video image processing (video-enhanced microscopy and video-intensified fluorescence microscopy) increases contrast and improves detection, but does not completely circumvent this limitation [3]. This problem can, however, be resolved by the use of confocal laser scanning microscopy (CLSM).

1.1. Advantages and disadvantages of CLSM

CLSM has become a well-established technique for obtaining high-resolution images (lateral, ~140 nm; axial, ~1 μm) from biological and other specimens. The major technical advantages of CLSM include (i) the ability to obtain images of optical sections with reasonable time-resolution in a non-invasive manner both in in vitro and in vivo conditions [6] (e.g. 10 s to acquire a good quality image), and (ii) visualization of images parallel to the surface of the sample, at multiple depths, without mechanical sectioning of the sample.

* Corresponding author. Section de Pharmacie, Faculté des Sciences, Université de Genève, 30, quai E. Ansermet, CH-1211 Genève 4, Switzerland. Tel.: +33-450-31-50-21; fax: +33-450-95-28-32.
E-mail address: richard.guy@pharm.unige.ch (R.H. Guy).

0939-6411/$ - see front matter © 2004 Elsevier B.V. All rights reserved.
doi:10.1016/j.ejpb.2004.03.027

Table 1
Lasers commonly used for confocal microscopy and the associated excitation lines

Laser	Output power (mW)	Monochromatic beam emitted (nm)
Argon ion	25–50	488 (blue), 514 (green)
	100	457 (blue), 488, 514
	250	351 (violet), 363 (violet), 488, 514
Krypton–argon ion	15–60	488, 568 (yellow), 647 (red)
Helium–neon	1	543 (green)
	10	595 or 633 (red)
Helium–cadmium	1-50	325 or 442 (blue)

The main limitation of CLSM resides in the range of lasers for which efficient fluorophore excitations can be achieved (see Table 1 for a comparison of the different lasers used in CLSM [7,8]). Also, exposure to the high-intensity laser illumination can be highly destructive to both viable tissue and the fluorophore itself, the latter being manifested as photobleaching in the x, y and z planes [9]. Another possible problem of CLSM is the autofluorescence of biological samples. Ideally, therefore, CLSM optically sections thick tissues that are sufficiently transparent to the laser excitation and fluorescence emission wavelengths, that do not strongly scatter this light, and are relatively free of autofluorescence [6].

Other difficulties are more specific to biological sample visualization. The sample induces spherical aberration when focusing through an interface between materials of different refractive indexes (RI), for example, between the immersion medium, the coverglass, and the sample [10]. The focal plane of the objective is deviated if a spherical structure with an RI different from that of the surrounding medium (RI_1) is introduced into the optical path. The focal plane moves upward when $RI > RI_1$ or downward when $RI < RI_1$. When the refractive index of the spherical structure is the same as the surrounding medium (RI_1), the focal plane of the objective remains on the mirror surface [11]. In general, aberrations cause a reduction in lateral resolution and, more significantly, degrade the axial resolution and cause a fall in signal intensity [12].

In addition, cellular components and the hydration state of the skin may introduce further aberrations and obstruct the adjustment of the 0-point of the skin surface. A CLSM study examining the depth-dependent spherical aberration in human skin concluded that if skin is imaged without a coverglass, the signal intensity can partially correct for the aberrations introduced by the layers of the skin [13].

1.2. Principles of confocal microscopy

In conventional microscopy, much of the depth or volume of the specimen is uniformly and simultaneously illuminated as well as the plane in which the objective lens is focused (Fig. 1A). This leads to out-of-focus blur from areas above and below the focal plane of interest. Out-of-focus light reduces contrast and decreases resolution, making it difficult to discern cellular structures. In contrast, the illumination in confocal microscopy is not simultaneous, but sequential [3]. The illumination is focused as a spot on one volume element of the specimen at a time (Fig. 1B). To achieve confocal imaging, excitation light from a laser scanning confocal microscope is directed towards the specimen. The beam of light passes through a scanning system and reaches the objective, which focuses the scanning beam as a spot on the specimen.

Fluorescence emission generated by the specimen scatters in all directions. Fluorescence from the focal plane of the specimen returns via the objective and scanning system, and is reflected off the dichroic mirror and focused onto a detector. In front of the detector is a spatial filter containing an aperture (pinhole diaphragm or slit), which defines the image of the spot in the focal plane of the microscope. Thus the spatial filter not only provides continuous access to the detector for in-focus light, but also effectively suppresses light from nonfocal planes [14]. A simplified diagram of the operating principle of CLSM is shown in Fig. 2.

1.2.1. z-Series

To obtain three-dimensional information from the skin, it is common practice to acquire a series of optical sections, referred to as a z-series, taken at successive focal planes along the z axis. The principle of z series acquisition is demonstrated schematically in Fig. 3.

Additionally, to obtain three-dimensional information from the z-series, individual slices of optical sections may be viewed as a simple image.

1.2.2. xz-Section

To obtain depth information from a specific surface, it is first necessary to acquire a confocal image in the xy-plane (i.e. parallel to the plane of the membrane surface).

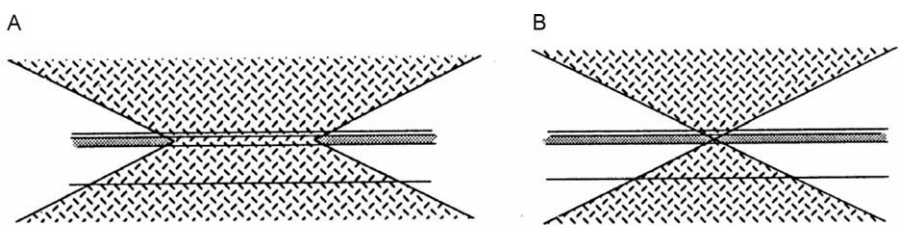

Fig. 1. Comparison between: (A) conventional fluorescence microscopy; and (B) confocal laser scanning microscopy. Redrawn from Ref. [14].

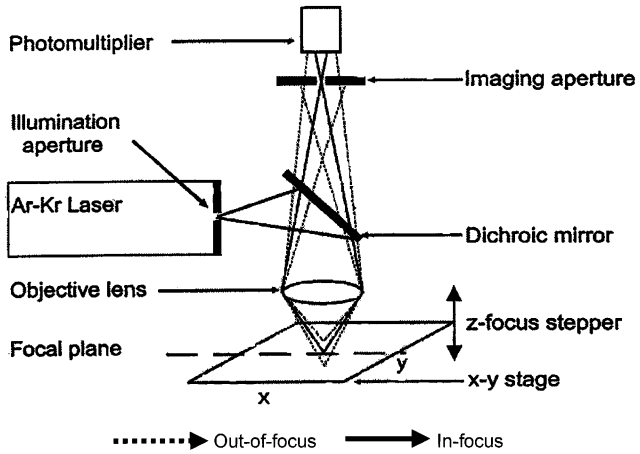

Fig. 2. Schematic diagram of the principle of confocal laser scanning microscopy. Redrawn from Ref. [9].

To generate an *xz*-section, a horizontal line is 'drawn' across a region of interest in the $z = 0$ μm-*xy*-plane and is then 'optically sliced' through the digitized image data of the successive *xy*-sections; the results are (*xz*-planar) optical cross-sections. Fig. 4 shows the principle of *xz*-planar optical cross-sectioning.

2. Applications of CLSM

2.1. Visualization of skin structures

CLSM provides valuable additional morphological information to that obtained from conventional microscopy. Simonetti et al. [15] characterized the barrier properties of reconstructed human epidermis by comparing the penetration pathways of fluorescent compounds (nile red and propidium iodide) across its stratum corneum (SC) with those across native tissue. Native and reconstructed epidermis were fixed and processed by embedding in paraffin. The images obtained by CLSM were also normalized to correct for (a) the influence of different vehicles on fluorescence intensity, and (b) the absorption and/or scattering of the exciting and emitted light deeper in the skin. The presence of intensely stained, round structures, suggesting the presence of multiple nuclei, was revealed following topical application of propidium iodide to reconstructed epidermis. In contrast, in hematoxylin–eosin stained tissue, cell nuclei could not be perceived by conventional light microscopy. CLSM is therefore a valuable tool for the rapid evaluation of the quality of reconstructed epidermis.

CLSM furthermore allows skin structure to be studied in three dimensions with very high accuracy. Vardaxis et al. [16] combined a fluorescent immunoassay and CLSM to obtain morphological information regarding the epithelial vascular supply, the hair follicle, and the density and arrangement of elastic fibres in the dermis. CLSM, in association with immunofluorescence, provided a clearer and sharper imaging method compared to conventional epifluorescence in studies involving skin injury and dermal healing [9,17].

Assessment of the distribution and abundance of microfibrils at the human dermal–epidermal junction has involved visualization using CLSM in association with an

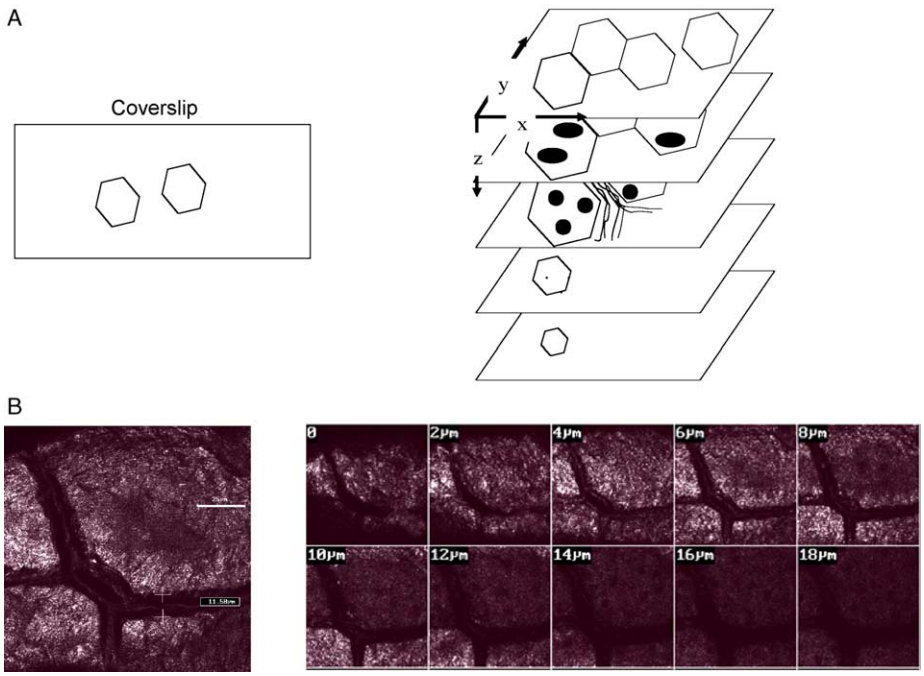

Fig. 3. Confocal optical sectioning I: (A) a schematic of a *z*-series (sequential *xy* sections as a function of depth (*z*)), and (B) confocal images of a *z*-series through porcine skin.

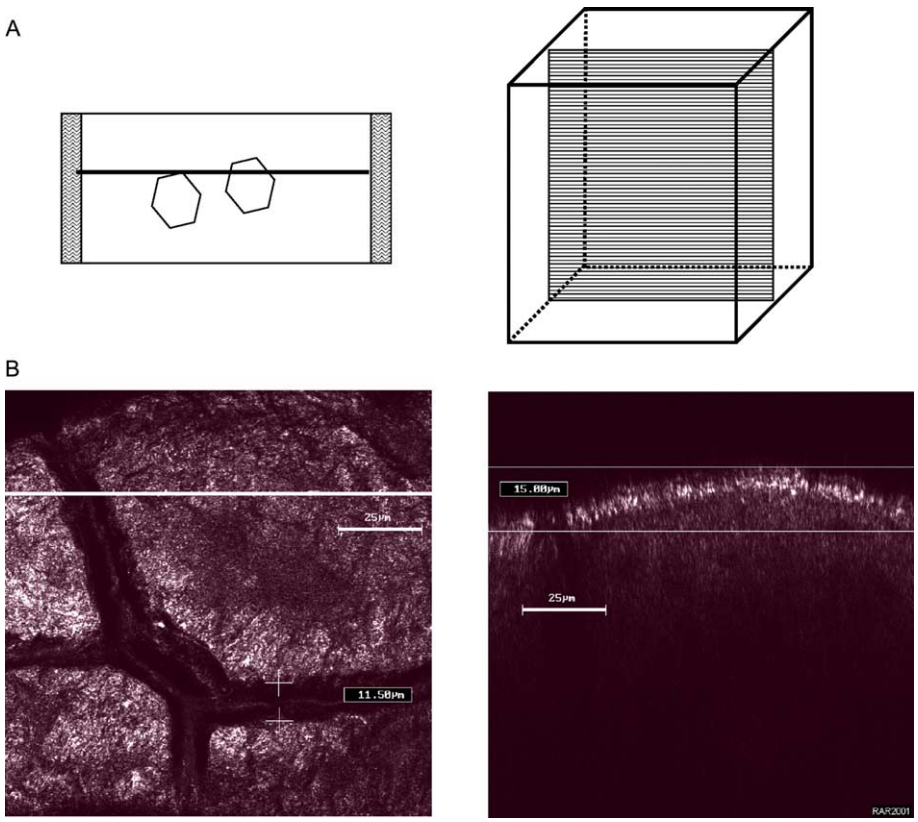

Fig. 4. Confocal optical sectioning II: (A) schematic of an *xz*-planar optical cross-section, and (B) a confocal *xz*-image of porcine skin.

immunofluorescence approach [18]. Watson et al. [19] examined the distribution and abundance of fibrillin-rich microfibrils, key structural components of the elastic fiber network, in photoaged and photoprotected skin. Punch biopsies taken from the arms of 16 subjects were fixed, dehydrated and delipidized prior to immunochemical staining for in situ elastin and fibrillin. This study demonstrated a markedly disrupted and reduced elastic fiber network in both minimally and severely photoaged skin. The loss of elastin or fibrillin fiber integrity in the upper dermis may contribute to the appearance and reduced elasticity of photoaged skin. In general, CLSM greatly improves the resolution of elastic fiber images [20].

CLSM is a useful technique for imaging thin sections with high contrast within an optically turbid object; moreover, the imaging is non-invasive and does not require the sample preparation necessary for conventional microscopy or routine histology. Boderke et al. [21] localized and visualized aminopeptidase activity within freshly dermatomed human skin with minimal perturbation of tissue integrity. The study was based on the visualization of a released fluorescent metabolite (rhodamine-110) subsequent to cleavage of a non-fluorescent, synthetic, aminopeptidase substrate, bis-Leu-rhodamine 110. Analysis of the images revealed that aminopeptidase activity in the skin was evenly distributed throughout the viable epidermis, with some enhancement in the upper stratum granulosum; the dermis and SC showed considerably less aminopeptidase activity. The fluorescence intensity appeared to be highest in the region immediately surrounding the hair (the root sheath), indicating particularly significant aminopeptidase activity in this area (Fig. 5).

CLSM has also been used to determine the distribution of a fluorophore in hair follicles [22]. The relative accumulation in the SC, epidermis, dermis, outer root sheath, inner root sheath, cuticular area and hair shaft in non-fixed fresh human scalp skin was determined semi-quantitatively. Using this approach, the relative accumulation of fluorophores of different lipophilicity, for example, could be compared. It was also possible to evaluate the effect of the vehicle on the disposition of the fluorophore within the skin [23], and it was found that delivery to the hair follicle could be improved by moderately increasing the penetrant's lipophilicity (Table 2).

Further, the effect of propylene glycol on the penetration rate and distribution of a series of fluorescent dyes with similar molecular weights, but varying lipophilicity, was studied in human scalp skin [34]. Follicular accumulation increased with increasing dye lipophilicity and propylene glycol incorporation in the formulations (Fig. 6).

It is possible to analyse certain biological specimens with CLSM utilising endogenous substances in the tissue that autofluoresce upon excitation [24]. Each fluorophore has a characteristic excitation and emission wavelength, a feature that facilitates its localization and quantification (Table 3).

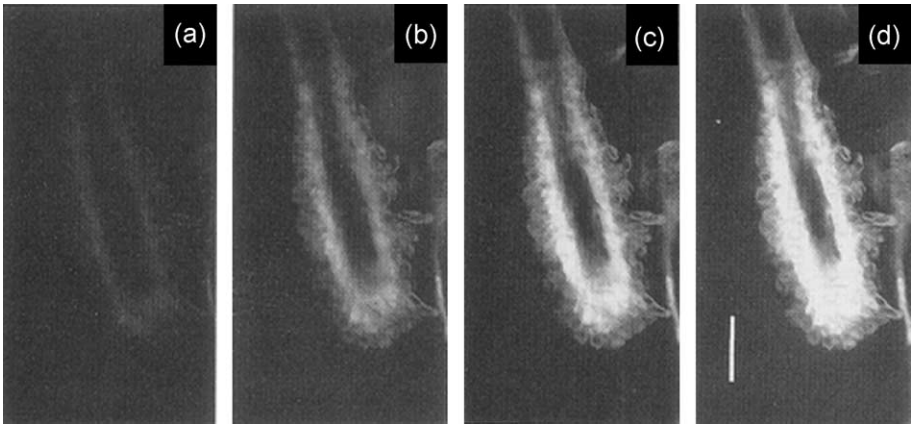

Fig. 5. Confocal micrographs of aminopeptidase activity in a hair follicle. The bottom surface of the sample was treated with Leu2-R110. Optical sections were taken after (a) 2, (b) 8, (c) 14, and (d) 20 min. The root sheath is notably fluorescent. Scale bar, 50 μm. Redrawn from Ref. [21].

Skin autofluorescence has been used to better understand the general functions of skin, for example, the formation of an essentially water-tight barrier by the intercellular lipids of the SC. Full-thickness human SC was visualized using its autofluorescence at a wavelength of 488 nm [35], and the increase in SC thickness after incubation in distilled water was determined.

SC swelling was approximately 25–30% in the vertical (thickness) dimension, but only 3–5% in the lateral (length) dimension. A comparison between delipidized and intact SC revealed that SC swelling is linked to the intercellular lipid structure and, hence, to skin barrier function. The recording of swelling in the vertical dimension in this study utilized the optical sectioning capability of CLSM [13].

It should also be mentioned that CLSM has also been used to study cutaneous nerves. Innervation patterns of epidermal nerves in various racial groups have not shown any significant differences [36], for example. Similarly, CLSM has been employed to determine follicular innervation differences in normal and diseased skin [37], the innervation of human cutaneous melanocytes [38], the innervation and vasculature of human sweat glands [39], the structure of human Meissner corpuscles [40] and Merkel complexes [41], and cutaneous nerve reinnervation patterns [42,43].

2.2. Visualization of skin in vivo

In the last decade, in vivo human skin imaging has been performed using a tandem scanning confocal microscope (TSCM), which operates in real-time and typically uses a bright mercury lamp [44,45]. However, only relatively few studies have examined skin autofluorescence in vivo, for example, the imaging of nuclear- and cellular-level detail in human skin [27]. Cellular features reported included cell diameter, nucleus diameter, inter-nucleus spacing, nuclear/cytoplasm ratio and cell (or nuclear) density within the granular, spinous, and basal layers of the epidermis of normal skin, vitiliginous skin, and in a compound nevus. Melanin provided strong contrast with visible light of 400–700 nm and the cellular and morphologic features determined confocally agreed well with those from the hematoxylin and eosin sections. CLSM of live human skin was possible in ‘real-time’, and provided high resolution, instantaneous, and non-destructive reflectance images of the epidermis and papillary dermis. This capability could be useful for instant clinical-pathologic correlations, diagnoses, and intraoperative tumour localization without biopsy and histology processing [46].

Subsequently, the resolution, contrast, depth of imaging, and field of view were improved [47] using longer near-infrared wavelengths (800–1064 nm), modified objective lenses (air immersion objectives for SC and water immersion lenses for viable, hydrated epidermis and dermis) with a range of magnifications and numerical apertures (0.7–1.2), and longer working distances, an extended range of pinhole sizes, and variable imaging rates. Melanin was the main chromophore for visible and near-infrared light, and granular, spinous and basal cell layers were visualized [27]. Other studies [13,44] have suggested that SC can be better

Table 2
Relative fluorescence (F_{rel}) (mean ± SE; $n = 3–4$) in the non-follicular (statum corneum, epidermis, dermis) and the follicular area (outer root sheath, inner root sheath, cuticle, hair shaft) after 18 h of diffusion of OG, BFL and B564 in either citric acid buffer (CAB) or CAB containing 30% (v/v) of ethanol (CAB-EtOH)

	F_{rel} (non-follicular, %)	F_{rel} (follicular, %)	log $P_{oct-CAB}$[a]
OG in CAB	94.4 ± 1.5	5.6 ± 1.5	1.6
OG in CAB-EtOH	90.5 ± 1.0	9.5 ± 1.0	1.6
BFL in CAB-EtOH	92.0 ± 0.4	8.0 ± 0.4	2.5
B564 in CAB-EtOH	87.6 ± 0.9	12.4 ± 0.9	4.3

OG, Oregon Green® 488; BFL, Bodipy, FL $C_5^®$; B564, Bodipy 564/570 $C_5^®$. The F_{rel} is a means to estimate how much of the calculated fluorescence is present in the follicular area compared to the non-follicular area in an assumed skin block [23].

[a] $P_{oct-CAB}$ = octanol − CAB partition coefficient.

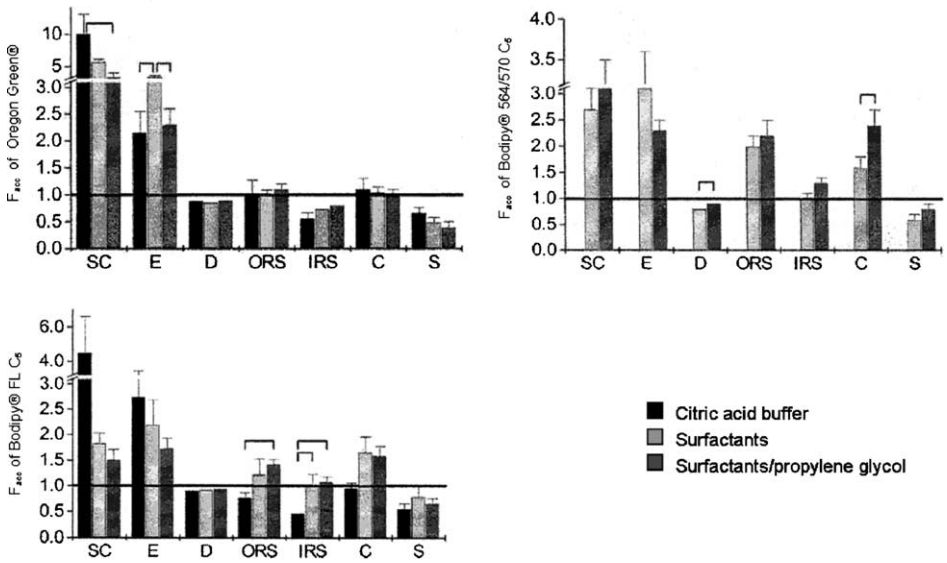

Fig. 6. Relative accumulation (F_{acc}) of Oregon Green® 488, Bodipy, FL C5®, and Bodipy® 564/570 C5 in the stratum corneum (SC), epidermis (E), dermis (D), outer root sheath (ORS), inner root sheath (IRS), cuticle (C), and hair shaft (S). The donor phase consisted of a saturated dye solution in either citric acid buffer (CAB), CAB containing 8% (w/v) surfactant, or CAB containing 8% (w/v) surfactant/20% (w/v) propylene glycol. Significant differences between pairs of values ($P < 0.05$) are indicated by horizontal bars. Redrawn from Ref. [34].

visualized by an immersion oil objective lens, which has the advantage that the refractive index of immersion oil (1.52) is closer to that of the SC. This minimizes spherical aberration and consequently increases the resolution. While histological images provide additional insight to that obtained with CLSM, the dark outlines of the corneocytes and the surface microtopography that are prominent in vivo, are not seen in hematoxylin and eosin-stained sections.

Recently, CLSM, using a miniaturized handheld scanner in combination with an exogenous fluorophore was also used to visualize intact living human skin. Swindle et al. [48] characterized the microscopic morphology of normal human epidermis in vivo after intradermal administration of fluorescein sodium. The images obtained by CLSM were recognizable and were consistent with histologic skin sections viewed by conventional microscopy. However, certain features could not be identified with confidence in the absence of complementary histological studies.

2.3. Improved skin delivery by chemical enhancement

PDT is a cancer treatment which uses a photosensitizer targeted to a tumour where it can produce tissue destruction by absorbing an adequate dose of light of appropriate wavelength [33]. The prodrug, 5-aminolevulinic acid (5-ALA), is converted in situ, on exposure to radiation, by the heme biosynthetic pathway, into a highly fluorescent substance, protoporphyrin IX (Pp-IX). The influence of DMSO and EDTA on 5-ALA-induced Pp-IX accumulation has been visualized by CLSM [33]. Following in vivo treatment, examination of excised mouse skin showed increased red fluorescence that was attributed to Pp-IX accumulation. However, because the excitation wavelength (478 nm) used may also excite autofluorescence in the skin (Table 2), additional controls are warranted before unambiguous interpretation of these results can be made.

2.4. Iontophoresis

Iontophoresis is the application of a low electrical potential gradient across the skin to enhance molecular transport [49]. To better understand the pathways involved, the iontophoretic permeation of fluorescent molecules with different physicochemical properties was investigated [50]. CLSM with dual-channel imaging was used to visualize, in hairless mouse skin, the distribution of calcein, a charged

Table 3
Endogenous substances responsible for the skin's autofluorescence

Fluorochrome	$\lambda_{excitation}$ (nm)	$\lambda_{emission}$ (nm)	Reference
Aromatic amino acids			
Tryptophan	295	345	[24,25]
Tyrosine	275	300	[25]
Phenylalanine	260	280	[26]
Structural proteins			
Melanin	330–380	400–700	[27]
Keratin	375	430	[28]
Collagen	335	390–405	[24,29]
Elastin	360	460	[24,29]
Enzymes and coenzymes			
FAD[a]	390	520	[30]
NADH[b]	290, 364	440, 475	[31]
NADPH[c]	336	464	[26]
Flavoprotein	450–490	500–560	[32]
Porphyrins	476	625	[30,33]

[a] Flavin adenine dinucleotide.
[b] Reduced nicotinamide adenine dinucleotide.
[c] Reduced nicotinamide adenine dinucleotide phosphate.

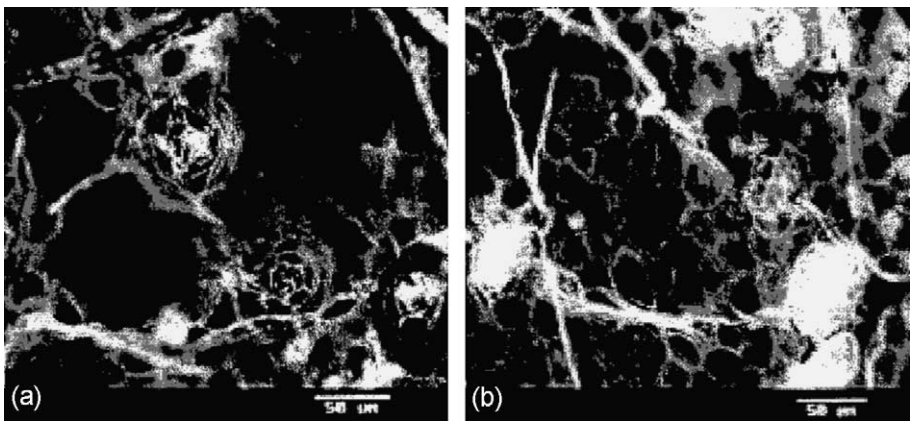

Fig. 7. $x-y$ Images obtained following (a) passive diffusion of nile red for 4 h, and (b) iontophoresis of nile red for 4 h. Confocal images were obtained (nominally) at 10 mm below the skin surface. Magnification 40 ×. Redrawn from Ref. [50].

(-4), hydrophilic dye, and nile red (NR), a lipophilic, neutral compound. The passive and iontophoretic delivery of NR occurred, as expected, via the lipid-filled intercellular regions of the SC; NR also sought out the lipid membranes of the epidermal keratinocytes. This is consistent with other studies, which have found NR to be an excellent stain for intracellular lipid droplets in biological tissues [15,51,52]. On the other hand, while the passive permeation of calcein was negligible, it was greatly enhanced, particularly in the follicular regions, by the application of an electrical potential (Fig. 7). This result confirmed that the appendageal pathway is a predominant route of iontophoretic transport for charged species [53]. Importantly, therefore, this study showed clearly that the iontophoretic pathway depends upon the physicochemical properties of the permeant.

In further work, a CLSM imaging procedure for the visualization and simultaneous quantification of a model, anionic, fluorescent compound (calcein) in skin was developed [54]. Full-thickness hairless mouse skin was examined by both optical and mechanical cross-sectional imaging. The approach was used to calculate the relative fractions of follicular and non-follicular transport [54]. As before, iontophoresis enhanced calcein delivery, particularly via the follicles, although non-follicular transport was also apparent, especially at more superficial levels.

The distribution of the detected fluorescence emphasized the importance of appendageal transport, especially when the data were normalized to take into account the relative areas of the follicular and non-follicular regions of the skin (Fig. 8). It should be emphasized that the quantification here

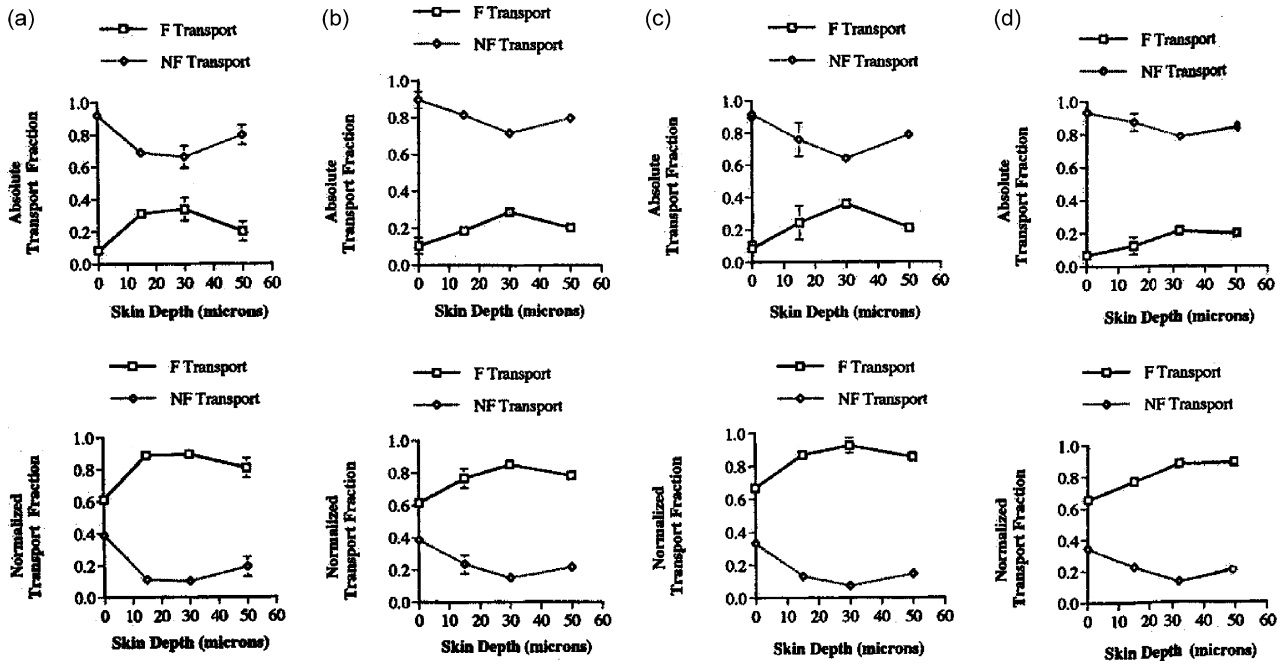

Fig. 8. Calcein transport via follicular (F) and non-follicular (NF) pathways following cathodal iontophoresis for (a) 1, (b) 2, (c) 4, and (d) 8 h, as a function of skin depth. Absolute (upper) and normalized (lower) transport was calculated from the corresponding CLSM images. Redrawn from Ref. [54].

is, at best, only relative and the intensities of fluorescent emission cannot be directly related to concentration (due to signal attenuation from the deeper skin layer). Note that this type of quantification can only be performed when the relationship between fluorophore concentration and fluorescent emission is linear [55].

Turner et al. [56] also studied the extent and distribution of iontophoretic skin penetration as a function of molecular weight of a series of model cationic peptides (poly-L-lysine, PLL) coupled to the fluorescent probe, FITC. Post-iontophoresis biopsies of hairless mouse skin were visualized by CLSM without fixation. Quantitative analysis of CLSM images revealed that iontophoresis increased transport via follicular pathways only slightly more than that through non-follicular regions for the 4 and 7 kDa FITC-PLL. However, transport of the 26 kDa substrate was not detectable even under iontophoretic conditions.

The skin penetration of fluorescent antisense oligonucleotides has also been studied using CLSM [57]. Regnier and Preat [58] studied the localization of a fluorescent oligodeoxynucleotide complex (FITC-ODN) in hairless rat skin, using fluorescence microscopy (FM) and CLSM, after topical delivery by iontophoresis and electroporation. Skin samples were directly examined by CLSM again without mechanical sectioning or fixation. The fluorescent images obtained by FM suggested that the pathways of FITC-ODN penetration in SC were paracellular during iontophoresis and transcellular during electroporation. In contrast, in this study, the CLSM images did not allow interpretation of the fluorescence localization of FITC-ODN in SC because these images were acquired at depths of approximately 20 μm below the surface, i.e. from the viable epidermis. Also, as hair follicles were not visualized by either FM or CLSM, it was impossible to confirm the role of the appendageal pathway for ODN.

More recently, a procedure to visualize and quantify the iontophoretic transport [54] of an ODN complex with polyethylenimine (PEI) was reported [59]. Human skin was cryofixed, embedded, sectioned and stained prior to its visualization by CLSM. The results demonstrated that non-complexed ODN could penetrate the skin after iontophoresis but not by passive diffusion.

CLSM has been also utilized to evaluate and visualize the influence of charged enhancers on iontophoretic transport through human skin in vitro. The transdermal delivery of dextran labelled with a fluorescent dye (Cascade Blue) under passive or iontophoretic conditions following pre-treatment with C12-penetration enhancers (sodium dodecyl sulphate, SDS, or dodecyltrimethylammonium bromide, DDTAB), has been studied [60]. The results demonstrated that use of a positively charged enhancer (DDTAB) improved the dextran penetration during passive and iontophoretic delivery. In an investigation comparing the passive and iontophoretic penetration of fluorescent lipids and stearylamine (in 32% ethanol) into the epidermis [61], confocal images revealed that ethanolic stearylamine penetrated across the entire epidermal layer during the 24 h pre-treatment of the skin. Without ethanol, only slight fluorescence was observed on the surface of the skin treated with lipid or stearylamine.

2.5. Electroporation

Electroporation is the application of short (a few milliseconds) high-voltage pulses to permeabilize a membrane (including the skin) thereby enhancing molecular transport [62]. The distribution of calcein across human skin was studied by CLSM subsequent to electroporation with low and high voltage pulses [63]. Regions of enhanced calcein fluorescence were induced by both moderate (40–75 V) and high (300 V) voltage pulsing across the skin. Transport pathways across the SC were inter- and trans-cellular. The latter were small, localized and brightly fluorescent areas that were not associated with appendages (Fig. 9).

The skin permeation of fluorescent FITC-dextran (MW ~ 38 kDa) was visualized after electroporation [64]. The FITC-dextran was detected in the epidermis, both around, and within the cytosol of the keratinocytes [58]. This suggests that high voltage pulses permeabilized both SC and the viable keratinocytes. Control experiments with FITC alone confirmed that the fluorescent label remained associated with dextran during the electroporation method.

2.6. Sonophoresis

Sonophoresis, the application of ultrasonic energy, is another physical approach to enhance percutaneous penetration. The importance of various mechanisms, including cavitation, thermal effects, generation of convective velocities and mechanical effects, in the ultrasonic enhancement of transdermal drug delivery has been evaluated [65].

Human epidermis was exposed to low frequency ultrasound in the presence of FITC and was then examined by CLSM. In the non-treated controls, the characteristic hexagonal structure of the corneocytes was visualized bounded by bright, continuous borders (the intercellular lipid domains). With ultrasound, on the other hand, fluorescence bleaching was observed and was postulated as being due to the oxidation of FITC by hydroxyl radicals produced after collapse of cavitation bubbles in an aqueous medium. It was concluded, therefore, that cavitation-mediated enhancement mechanism plays a key role in sonophoresis.

More recent investigations compared the effects of low- and high-frequency ultrasound [66,67] on skin permeation. Only low frequency ultrasound (20 kHz) resulted in significantly increased permeation, and it again appeared that cavitation was principally responsible for the lowered skin barrier function observed (although perhaps as much as 25% of the effect could be attributable to the increased temperature induced by ultrasound). Subsequent

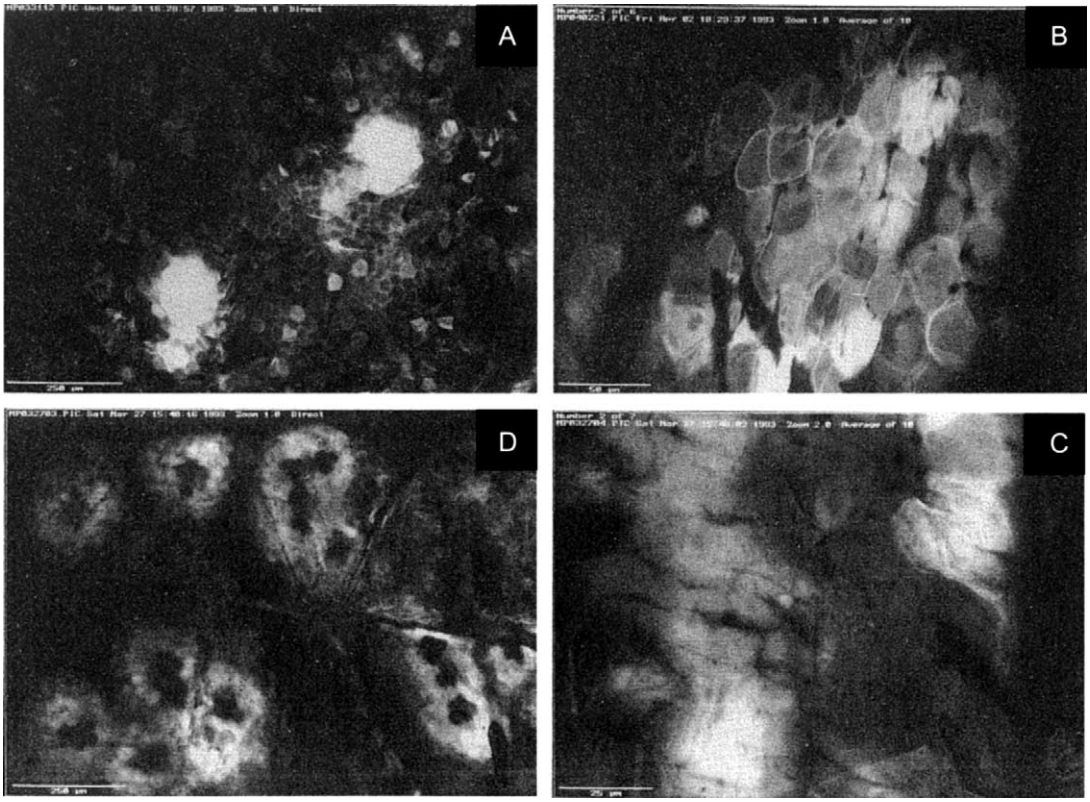

Fig. 9. Calcein fluorescence in human stratum corneum following electroporation at 40–75 and 300 V. (A) A low-magnification section after pulsing at a transdermal voltage of 75 V. (B) High-magnification sections at − 5 mm after pulsing at 40 V. Transport appears to have occurred through intercellular and/or localized transcellular pathways. (C) High-magnification sections after pulsing at a transdermal voltage of 300 V. (D) High-magnification sections at − 5 mm after pulsing at 300 V. Transport appears to have occurred via intercellular and/or transcellular routes at localized, ring-like sites. Redrawn from Ref. [63].

experiments [68] using nile red and calcein as lipophilic and hydrophilic model permeants, respectively, showed that sonophoresis induced localized regions of increased skin permeability (i.e. that there was not a generalized lowering of skin barrier function over the entire treated surface). This effect was consistent with earlier findings [67] and with a cavitation-based mechanism. Not surprisingly, the opening of essentially hydrophilic pathways across the skin in this way had a much greater impact on the transport of calcein as compared to nile red (Figs. 10 and 11).

2.7. Vesicle-mediated skin transport

Encapsulation of drugs in phospholipid vesicle suspensions (liposomes) has attracted considerable attention as a novel strategy for topical drug delivery [69].

Generally speaking, three principal mechanisms can be envisaged for the vehicle-mediated skin uptake of an associated penetrant:

(i) the intact vehicle transports across the skin carrying its ‘payload’ with it.
(ii) the vesicle dissociates at or near the skin surface and then the penetrant is absorbed in association with fragments (or constituents) of the carrier; and
(iii) post-application to the skin, the penetrant partitions rapidly from the vehicle into the SC and crosses the barrier alone [70,71].

Clearly, the second and third mechanisms also allow for the possibility that vesicle components may themselves permeate the membrane and even disrupt its barrier function (i.e. they may act as penetration enhancers). Furthermore, it is conceivable that vesicles may break down and reform in situ incorporating thereby, for example, lipids originating from the skin surface (e.g. sebaceous lipids) or lipids from the intercellular domains of the SC.

Despite the importance of these mechanistic questions, however, CLSM has not been able to provide unequivocal confirmation of the precise details involved. Nevertheless, an examination of the relevant literature provides valuable information and insight. In an early experiment, the permeation of a free fluorescent marker was shown to occur primarily via the SC intercellular lipid pathway [70]. Subsequently, when the marker was administered in a series of liposomes of different compositions, it was not possible to determine whether the fluorescence observed in the CLSM images originated from encapsulated or free fluorophore [72].

Recently, the transport of carboxyfluorescein (CF)-loaded phospholipid liposomes across human skin was studied by

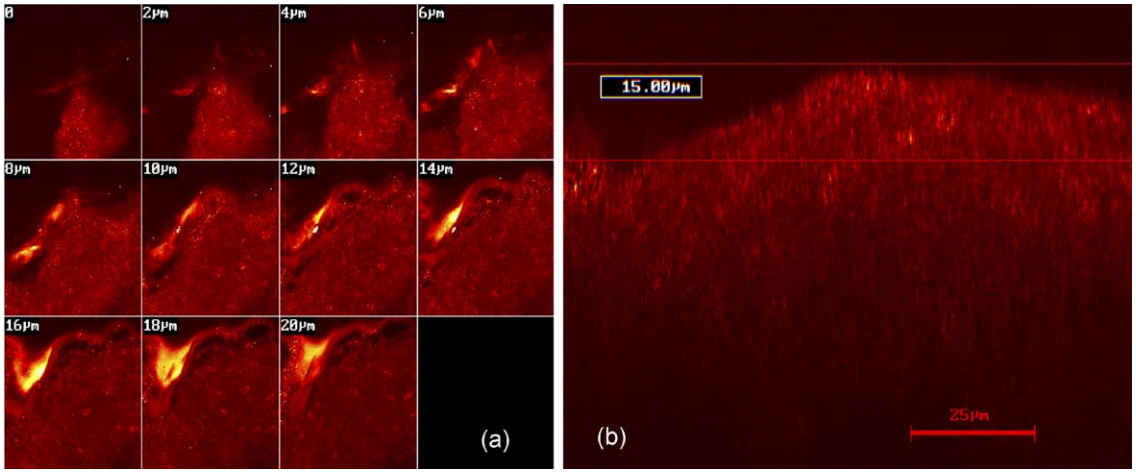

Fig. 10. Confocal images following 2 h of low-frequency sonophoresis of nile red. (a) A *z*-series from the surface of the SC (0 μm) to a depth of 20 μm. (b) An *xz* cross-sectional image. Scale bar, 25 μm. Redrawn from Ref. [68].

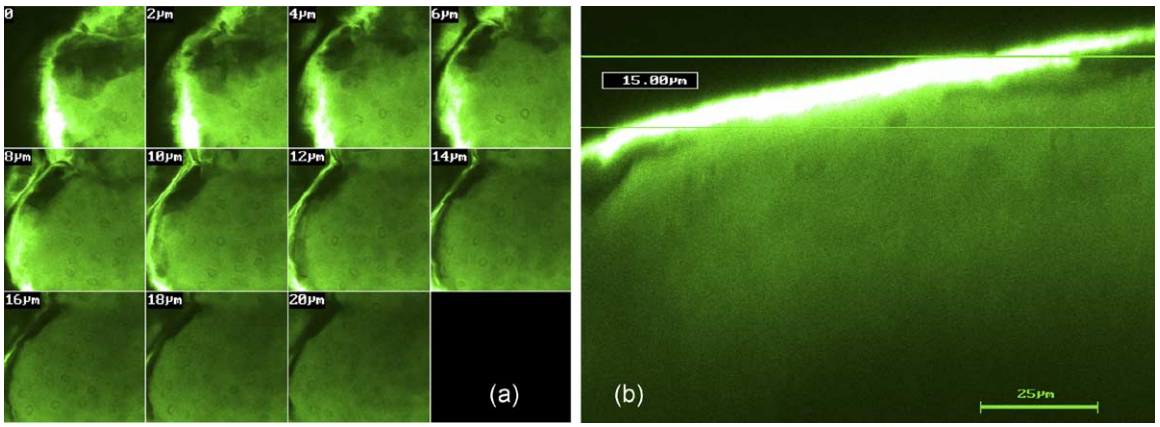

Fig. 11. Confocal images following 2 h of low-frequency sonophoresis of calcein. (a) A *z*-series from the surface of the SC (0 μm) to a depth of 20 μm. (b) An *xz* cross-sectional image. Scale bar, 25 μm. Redrawn from Ref. [68].

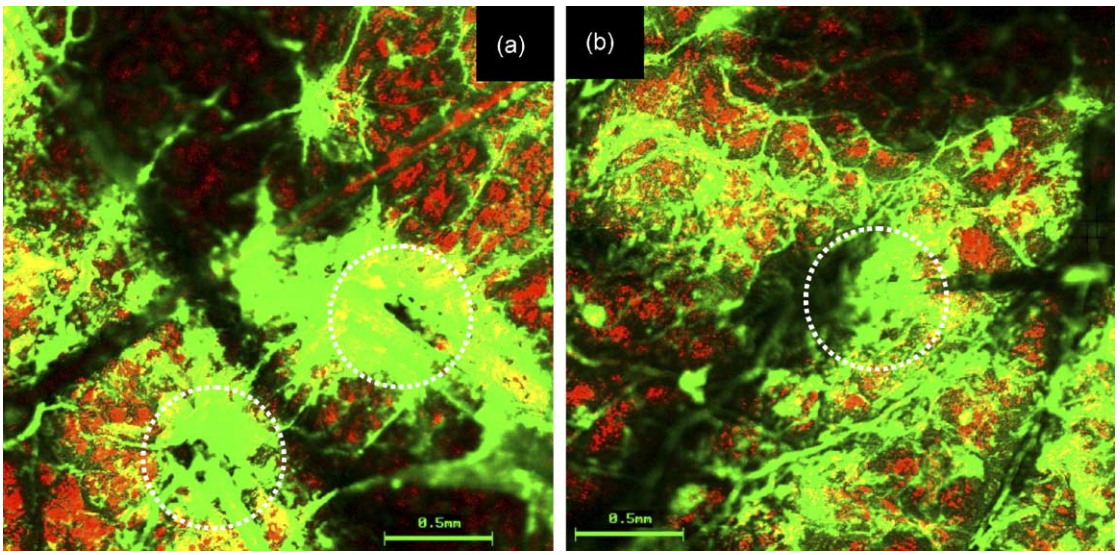

Fig. 12. *x*–*y* Images showing follicular localization of FITC-nanoparticles subsequent to a 2-h application of (a) 20 nm FITC-nanoparticles, and (b) 200 nm FITC-nanoparticles. Note that accumulation in the hair follicle is particularly apparent for the smaller nanoparticles. Scale bar, 500 μm [91].

Verma et al. [73]. The formulation containing CF both inside and outside the vesicles showed enhanced penetration of dye into the human SC as compared to the formulations containing the dye only outside the liposomes and in buffer alone, suggesting that the phospholipid vesicles are able to carry the entrapped as well as adsorbed dye into the SC and possibly into the deeper layers of the skin.

A CLSM study examining the penetration of phosphatidylcholine liposomes across human skin concluded that intact liposomes did not penetrate the skin [74]. Similar findings have been reported in the literature; for example, Kirjavainen et al. [75] demonstrated that fluorescent liposomes did not penetrate the skin when delivered from an aqueous solution, but penetrated to deeper regions from ethanolic solutions.

Several studies have emphasised the importance of liposomal size in skin penetration [76,77]. In a recent confocal study [78], the deposition of carboxyfluorescein from a series of liposomes (120–810 nm), across various strata of human abdominal skin, was found to be inversely related to the size of the liposomes.

CLSM has also been used to investigate the interaction of topically applied liposomes with reconstructed human epidermis [15]. For example, Zellmer et al. [79] studied the influence of liposome composition (phosphatidylcholine (PC), phosphatidylserine (PS) and human SC lipids (hSCL)). CLSM images indicated that PC liposomes appeared homogeneously dispersed within the reconstructed human epidermis, while PS and hSCL liposomes were aggregated on the tissue surface.

Recently, two novel vesicular carriers for enhancing drug penetration into the SC have been reported: ethosomes and transferosomes. Ethosomes are soft phospholipid vesicular systems incorporating water and ethanol in relatively high concentrations, the size of which can be modulated from tens of nanometers to microns [80]. The ability of ethosomes to deliver lipophilic molecules to the deep layers of the skin was investigated by CLSM [81,82]. An enhanced ethosome-mediated delivery of 4-(4-diethyl amino)styryl-*N*-methylpyridium iodide, in terms of depth and quantity, was reported. Transferosomes, ultradeformable phospholipid carriers, have also been shown to be versatile carriers for local administration [83]. The CLSM images indicated that the rhodamine from transferosomes was distributed uniformly over the skin [84].

Drug encapsulation is a useful pharmaceutical strategy for modifying the physicochemical properties of the encapsulated molecule and offers a means to facilitate the percutaneous delivery of difficult-to-deliver substances. Microspheres (>1 μm) and nanoparticles (<1 μm), which differ only in their size distribution, are commonly used polymeric systems in drug delivery.

To-date, CLSM studies investigating the interaction between nanoparticles and biological tissues include studies with rabbit ocular tissue [85,86], rabbit nasal respiratory mucosa [87] and rat intestinal epithelium [88]. The interaction of fluorescent biodegradable nanoparticles with porcine skin was visualized by CLSM [89]. Subsequent experiments [90] using nile red-containing nanoparticles showed that encapsulation increased fluorescence intensity across the SC. However, these experiments could not determine unequivocally whether the fluorescence observed in the CLSM images originated from the fluorophore associated with the nanoparticles or from free fluorophore (released from the nanoparticles). In order to better understand the mechanism by which such particulate

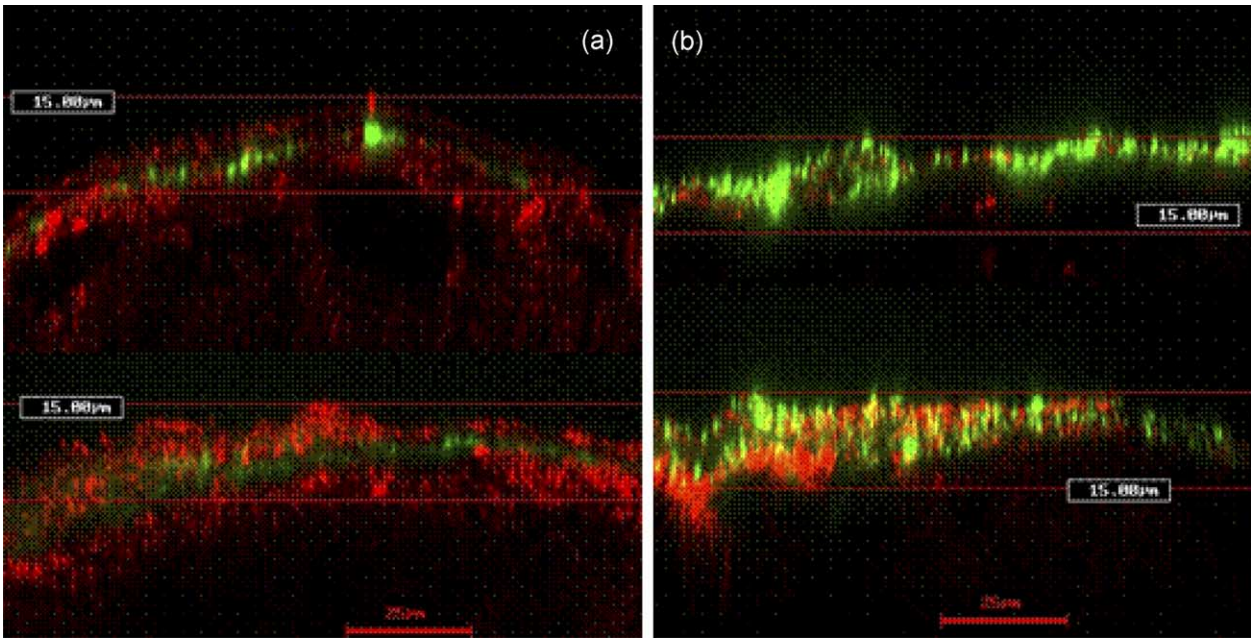

Fig. 13. $x-z$ Cross-sectional images obtained subsequent to a 2-h application of (a) 20 nm FITC-nanoparticles, and (b) 200 nm FITC-nanoparticles [91].

Table 4

Fluorescence probe	λ_{exc} (nm)	λ_{em} (nm)	Goal of study	Reference
Alexa-568-conjugate	568	605	Visualization of possible mechanism of skin penetration of oil/water emulsion containing a non-steroidal anti-inflammatory drug	[92]
Benzene[a]	325		Characterization of the stratum corneum lipid matrix	[93]
Bodipy FL C_5	488	514	Penetration and distribution of lipophilic probes in the hair follicle	[23,34]
Bodipy 564/570 C_5	564	574	Penetration and distribution of lipophilic probes in the hair follicle	[23]
CAELYX®-liposome (fluorescent drug encapsulated)			Distribution of fluorescent drug encapsulated in polyethylene-glycol coated liposome in frozen tumour sections	[94]
Calcein	488	510	Visualization of iontophoretic transport pathways of a multiply charged and hydrophilic molecule	[50]
	496	517	Mechanism of electroporation and iontophoresis using different animal skins as models for human skin	[4]
	495	512	Visualization and quantification of skin iontophoretic pathways	[54]
	488	510	Visualization of iontophoretic pathways in hairless mouse skin with CLSM and the vibrating probe electrode	[6]
	495	512	Visualization of skin transport pathways by low frequency sonophoresis	[68]
Cascade blue-dextran	401	431	Investigation and visualization of the passive and iontophoretic pathways across human stratum corneum	[60]
D-289[b]	488	527	Interaction of topically applied antiparkinsonian ethosomes whit skin	[82]
DAPI[c]	364	385	Visualization of skin transport properties of model molecule as a carrier for oligodeoxynucleotide (ODN) during iontophoresis and electroporation	[58]
DiI	578	590	Visualization of the effect of liposome particle size on dermal delivery of substances into skin	[78]
DSPC[d]	488	515	Visualization of the influence of lipids on the mannitol flux during transdermal iontophoresis	[61]
Ethidium bromide	510	595	Visualization of a topical application of novel liposome-plasmid DNA formulations in vivo	[95]
Fluorescein-carboxy-liposomes	488	515	Evaluation of the transport of fluorescent phospholipid liposomes across human skin	[73]
Fluorescein-DHPE[e]	488	515	Determination of penetration pathway and penetration depth of the lipophilic fluorescent label into the skin	[72]
	488	515	Visualization of interaction between liposomes and human skin in vitro	[70,71]
	496	519	Exploration of the three-dimensional structure, organization and barrier function of the SC ex vivo and in vivo after trensfersome permeation	[83]
Fluorescein-C_{18}[f]	488	515	Visualization of interaction between liposomes and human skin in vitro	[71]
	488	515	Visualization of interaction between liposomes and rat skin in vitro	[72]
FITC-oligonucleotides	488	515	Distribution of oligonucleotide or oligonucleotide-liposome complexes in human skin grafts on nude mice	[96]
FITC-oligonucleotides	488	515	Localization of oligonucleotide in the skin after topical delivery by iontophoresis and electroporation	[58]
FITC-dextran	488	522	Localization of macromolecule distribution after skin electroporation	[64]
FITC poly-L-lysine	488	520	Determination of the extent of iontophoretic transport in hairless mouse skin as a function of drug molecular weight	[56]
FITC-dextran, FITC-triglycine, FITC-sacharose			Visualization of small unilamellar liposome penetration into human skin	[97]
NBD-ceramide[g]			Visualization of Golgi apparatus of cultured keratinocytes	[98]
NBD-DPPE[h]			Visualization of small unilamellar liposome penetration into human skin	[97]
NBD-diethanolamine			Visualization of iontophoretic pathways in hairless mouse skin with CLSM and the vibrating probe electrode	[6]
Nile red	568	590	Visualization of iontophoretic transport pathways of a neutral and lipophilic compound	[50]
	551	630	Visualization of intercellular spaces at the stratum granulosum–stratum corneum interface	[98]
	568	590	Visualization of iontophoretic pathways in hairless mouse skin with CLSM and the vibrating probe electrode	[6]
	543	630	Visualization of skin transport pathways by low frequency sonophoresis	[68]
			Visualization of possible mechanism of penetration of oil/water emulsion containing a non-steroidal anti-inflammatory drug	[92]
	543	630	Visualization of possible mechanism of penetration of biodegradable polymer nanospheres into the skin	[89,90]
			Visualization of the lipid barrier and measurement of lipid pathlength in human stratum corneum	[99]
Oregon green 488	488	514	Penetration and distribution of lipophilic probes in the hair follicle	[23,34]
Oregon-green-polyethylenimine	488	505	Visualization of skin transport properties of model molecule as a carrier for oligodeoxynucleotide (ODN) during iontophoresis	[59]

(*continued on next page*)

Table 4 (*continued*)

Fluorescence probe	λ_{exc} (nm)	λ_{em} (nm)	Goal of study	Reference
Particle polymeric (carboxilate-modified polystyrene latex®)	470	505	Visualization of possible transport of highly charged particles across the skin by short high-voltage pulses	[100]
	488		Visualization of penetration and distribution of fluorescent nanoparticles into the skin	[91]
Particle polymeric (fluorescent drug encapsulated[i])	313	400	Visualization of site-specific fluorescent drug delivery to pilosebaceous structures using polymer microspheres	[101]
Protoporphyirine	476	590	Determination of in vivo protoporphyrin IX accumulation for photodynamic therapy of skin cancer	[33]
Rhodamine B base	524	580	Retention, permeability and penetration of charged multilamellar liposomes	[102]
	524	580	Visualization of PLGA microsphere in pig alveolar macrophages	[103]
Rhodamine B octadecyl	568	590	Visualization of the influence of lipids on the mannitol flux during transdermal iontophoresis	[61]
Rhodamine B sulfonyl	568	590	Visualization of liposome–skin interaction and their effects on the skin permeation of drug	[75]
Rhodamin-PE[j]	543	590	Interaction of topically applied fluorescent liposome with reconstructed epidermis	[79]
Rhodamine sulfo-	586	607	Mechanism of electroporation and iontophoresis using different animal skins as models for human skin	[4]
Rhodamine 110	492	523	Localization and direct visualization of aminopeptidase activity in human skin	[21]
Rhodamine-DHPE[k]	543	590	Exploration of the three-dimensional structure, organization and barrier function of the SC ex vivo and in vivo after trensfersome permeation	[83,84]
Rhodamine red	488	560	Interaction of topically applied antiparkinsonian ethosomes whit skin	[82]
	488	560	Evaluation of ability of ethosomes to deliver molecules to the deep layers of the skin	[81]
SNARF-1[l]	518 (acid)	535	Determination of the pH gradient across the stratum corneum	[104]
	538 (base)	635		
TAMRA-oligodeoxynucleotide	543	560	Visualization of skin transport properties of model molecule as a carrier for oligodeoxynucleotide (ODN) during iontophoresis	[59]
Texas Red-DHPE[m]	583	601	Exploration of the three-dimensional structure, organization and barrier function of the SC ex vivo and in vivo after trensfersome permeation	[83]

[a] 1,4-bis-(5-phenyl-2-oxazolyl)-benzene.
[b] D-289 = (4-(4-diethyl amino)styryl-*N*-methylpyridinium iodide).
[c] DAPI = 4′,6-diamidino-2-phenylindole.
[d] DSPC = 2-(12-7-nitrobentz-2-oxa-1,3-diazol-4-yl)-amino-dodecanoyl-1-hexadecanoyl-*sn*-glycero-3-phospho-choline.
[e] FI-DHPE = *N*-(5-fluoresceinthiocarbamoyl)-1,2-dihexadecanoyl-*sn*-glycero-3-phospho-ethanolamine.
[f] FI-C18 = *N*-octadecyl-*N*′-(5(fluoresceinyl))thiourea.
[g] NBD-ceramide = [6-(1*N*-(7-nitrobenz-a-oxa-1,3-diazol-4-yl)amino)-caproyl sphingosine.
[h] NBD-DPPE = (*N*-57-nitro-2,1,3-benzoxadiazol-4-yl)dipalmitoylphosphatidylethanolamine.
[i] Adapalene = Adapalene[6-(3-(1-adamantyl)4-methoxypehenyl)-2-naphthoic acid.
[j] Rhodamin-PE = 1,2-dipalmitoyl-*sn*-glycero-3-phospho-ethanolamine-*N*-rhodamine.
[k] Rhodamine-DHPE = 1,2-dihexa-adecanoyl-*sn*-glycero-3-phosphoethanolamine-*N*-Lis-samine.
[l] SNARF-1 = carboxyl seminaphthorhodafluor.
[m] Texas Red-DHPE = 1,2-dihexa-adecanoyl-*sn*-glycero-3-phosphoethanolamine-*N*-Lis-samine.

formulations enhance skin transport, the authors monitored, using CLSM, the distribution of non-biodegradable polystyrene fluorescent nanoparticles [91]. The use of non-biodegradable polystyrene nanoparticles containing covalently bound fluorophore ensured that the fluorescence detected by CLSM, originated from the nanoparticles. In doing so, the cutaneous localization of the selected nanoparticles, and the dependence of the distribution on particle size, was visually evaluated. These fluorescent nanoparticles, particularly the smaller particle size, accumulated preferentially in the follicular openings (Fig. 12). While nanoparticles were also found in 'furrows' on the skin, no evidence for uptake of the vectors away from the follicles was observed (Fig. 13).

3. Fluorescent probes used for visualizing skin

Table 4 is a comprehensive list of fluorophores commonly used in skin visualization.

4. Conclusions

Without question, CLSM has provided a significant tool with which to visualize skin structure and the localization of fluorescent probes within the tissue. Because of its non-destructive nature, and the fact that little or no sample preparation is necessary, CLSM offers a reasonably faithful representation of reality with few artefacts. The potential to

recreate three-dimensional visualization of the tissue is another significant advantage relative to other microscopic techniques. CLSM provides complementary image information to that obtained from other conventional microscopic and histological methods. The major contribution of CLSM in the topical/transdermal field to-date have been mechanistic, particularly in terms of revealing preferred penetration pathways following, the use of different delivery technologies. Nevertheless, there remain important limitations of CLSM. First, only a restricted range of fluorophores are available for imaging and attachment of these markers, for example, to a dry of interest may change significantly the permeability behaviour (rate, extent, route of transport, etc.). Second, the technique reveals at best only semi-quantitative information, and no approach to calibrate the fluorescence intensities observed has yet been demonstrated. Third, the images obtained are static views of reality captured at a particular point in time; thus, does a strongly fluorescent region imply a key pathway through which a large fraction of the total transport is occurring, or does it suggest an area where the fluorophore has become tightly bound and/or immobilized. Future work will undoubtedly address these, and other, important questions.

Acknowledgements

Rocío Alvarez-Román is the recipient of grant from CONACyT-SFERE, México-France.

References

[1] L.A. Pechtold, H.E. Boddé, H.E. Junginger, H.K. Koerten, J.A. Bouwstra, X-ray microanalysis of cryopreserved human skin to study the effect of iontophoresis on percutaneous ion transport, Pharm. Res. 18 (2001) 1012–1017.
[2] B.A. van den Bergh, J. Vroom, H. Gerritsen, H.E. Junginger, J.A. Bouwstra, Interactions of elastic and rigid vesicles with human skin in vitro: electron microscopy and two-photon excitation microscopy, Biochim. Biophys. Acta 1461 (1999) 155–173.
[3] S.J. Wright, V.E. Centonze, S.A. Stricker, P.J. DeVries, S.W. Paddock, G. Schatten, An introduction to confocal microscopy and three-dimensional reconstruction, in: B. Matsumoto (Ed.), Cell Biological Applications of Confocal Microscopy, Academic Press, USA, 1993, pp. 2–43.
[4] T. Chen, R. Langer, J.C. Weaver, Skin electroporation causes molecular transport across the stratum corneum through localized transport regions, J. Invest. Dermatol. Symp. Proc. 3 (1998) 159–165.
[5] V. Koprda, M. Harangozo, Z. Kassai, Transfer of radionuclides across skin barriers of animal skin models in vitro, J. Radioanal. Nucl. Chem. 246 (2000) 505–509.
[6] C. Cullander, R.H. Guy, Visualization of iontophoretic pathway with confocal microscopy and the vibrating probe electrode, Solid State Ionics 53–56 (1992) 197–206.
[7] K. Yamaguchi, Observation of microcirculatory kinetics by real-time confocal laser scanning microscopy, in: P.M. Conn (Ed.), Confocal Microscopy, Academic Press, Sydney, 1999, pp. 394–424.
[8] T.C. Brelje, M.W. Wessendorf, R.L. Sorenson, Multicolor laser scanning confocal immunofluorescence microscopy: practical application and limitations, in: B. Matsumoto (Ed.), Cell Biological Applications of Confocal Microscopy, Academic Press, USA, 1993, pp. 98–177.
[9] K.C. Pedley, Applications of confocal and fluorescence microscopy, Digestion 58 (Suppl 2) (1997) 62–68.
[10] R. Bacallao, K. Kiai, L. Jesaitis, Guiding principles of specimen preservation for confocal fluorescence microscopy, in: J.B. Pawley (Ed.), Handbook of Biological Confocal Microscopy, Plenum Press, New York, 1990, pp. 311–325.
[11] P.C. Cheng, A. Kriete, Image contrast in confocal light microscopy, in: J.B. Pawley (Ed.), Handbook of Biological Confocal Microscopy, Plenum Press, New York, 1990, pp. 281–310.
[12] M.J. Booth, M.A.A. Neil, J. Juskaitis, T. Wilson, Adaptive aberration correction in a confocal microscopy, Appl. Phys. Sci. 99 (2002) 5789–5792.
[13] M.J. Booth, T. Wilson, Strategies for the compensation of specimen-induced spherical aberration in confocal microscopy of skin, J. Microsc. 200 (2000) 68–74.
[14] D.M. Shotton, Confocal scanning optical microscopy and its applications for biological specimens, J. Cell Sci. 94 (1989) 175–206.
[15] O. Simonetti, A.J. Hoogstraate, W. Bialik, J.A. Kempenaar, A.H. Schrijvers, H.E. Boddé, M. Ponec, Visualization of diffusion pathways across the stratum corneum of native and in-vitro-reconstructed epidermis by confocal laser scanning microscopy, Arch. Dermatol. Res. 287 (1995) 465–473.
[16] N.J. Vardaxis, T.A. Brans, M.E. Boon, R.W. Kreis, L.M. Marres, Confocal laser scanning microscopy of porcine skin: implications for human wound healing studies, J. Anat. 190 (1997) 601–611.
[17] D. Salomon, E. Masgrau, S. Vischer, S. Ullrich, E. Dupont, P. Sappino, J.H. Saurat, P. Meda, Topography of mammalian connexins in human skin, J. Invest. Dermatol. 103 (1994) 240–247.
[18] M. Raghunath, M. Tschodrich-Rotter, T. Sasaki, M. Meuli, M.L. Chu, R. Timpl, Confocal laser scanning analysis of the association of fibulin-2 with fibrillin-1 and fibronectin define different stages of skin regeneration, J. Invest. Dermatol. 112 (1999) 97–101.
[19] R.E. Watson, C.E. Griffiths, N.M. Craven, C.A. Shuttleworth, C.M. Kielty, Fibrillin-rich microfibrils are reduced in photoaged skin. Distribution at the dermal–epidermal junction, J. Invest. Dermatol. 112 (1999) 782–787.
[20] H.F. de Carvalho, S.R. Taboga, Fluorescence and confocal laser scanning microscopy imaging of elastic fibers in hematoxylin-eosin stained sections, Histochem. Cell Biol. 106 (1996) 587–592.
[21] P. Boderke, H.P. Merkle, C. Cullander, M. Ponec, H.E. Boddé, Localization of aminopeptidase activity in freshly excised human skin: direct visualization by confocal laser scanning microscopy, J. Invest. Dermatol. 108 (1997) 83–86.
[22] Y.Y. Grams, J.A. Bouwstra, A new method to determine the distribution of a fluorophore in scalp skin with focus on hair follicles, Pharm. Res. 19 (2002) 350–354.
[23] Y.Y. Grams, J.A. Bouwstra, Penetration and distribution of three lipophilic probes in vitro in human skin focusing on the hair follicle, J. Control. Release 83 (2002) 253–262.
[24] N. Kollias, R. Gillies, M. Moran, I.E. Kochevar, R.R. Anderson, Endogenous skin fluorescence includes bands that may serve as quantitative markers of aging and photoaging, J. Invest. Dermatol. 111 (1998) 776–780.
[25] N. Kollias, G.N. Stamatas, Optical non-invasive approaches to diagnosis of skin diseases, J. Invest. Dermatol. Symp. Proc. 7 (2002) 64–75.
[26] N. Ramanujam, Fluorescence spectroscopy in vivo, in: R.A. Meyers (Ed.), Encyclopedia of Analytical Chemistry, Wiley, Chichester, 2000, pp. 20–56.
[27] M. Rajadhyaksha, M. Grossman, D. Esterowitz, R.H. Webb, R.R. Anderson, In vivo confocal scanning laser microscopy of human skin: melanin provides strong contrast, J. Invest. Dermatol. 104 (1995) 946–952.

[28] H.J.C.M. Sterenborg, M. Motamedi, J.R.F. Wagner, M. Duvic, S. Thomsen, S.L. Jacques, In vivo fluorescence spectroscopy and imaging of human skin tumours, Lasers Med. Sci. 9 (1994) 191–201.
[29] R. Gillies, G. Zonios, R.R. Anderson, N. Kollias, Fluorescence excitation spectroscopy provides information about human skin in vivo, J. Invest. Dermatol. 115 (2000) 704–707.
[30] R. Na, I.M. Stender, L. Ma, H.C. Wulf, Autofluorescence spectrum of skin: component bands and body site variations, Skin Res. Technol. 6 (2000) 112–117.
[31] D. Brotchie, N. Roberts, M. Birch, P. Hogg, C.V. Howard, I. Grierson, Characterization of ocular cellular and extracellular structures using confocal microscopy and computerized three-dimensional reconstruction, in: P.M. Conn (Ed.), Confocal Microscopy, Academic Press, Sydney, 1999, pp. 496–512.
[32] B.R. Masters, P.T. So, E. Gratton, Multiphoton excitation fluorescence microscopy and spectroscopy of in vivo human skin, Biophys. J. 72 (1997) 2405–2412.
[33] F.S. De Rosa, J.M. Marchetti, J.A. Thomazini, A.C. Tedesco, M.V. Bentley, A vehicle for photodynamic therapy of skin cancer: influence of dimethylsulphoxide on 5-aminolevulinic acid in vitro cutaneous permeation and in vivo protoporphyrin IX accumulation determined by confocal microscopy, J. Control. Release 65 (2000) 359–366.
[34] Y.Y. Grams, S. Alaruikka, L. Lashley, J. Caussin, L. Whitehead, J.A. Bouwstra, Permeant lipophilicity and vehicle composition influence accumulation of dyes in hair follicles of human skin, Eur. J. Pharm. Sci. 18 (2003) 329–336.
[35] L. Norlen, A. Emilson, B. Forslind, Stratum corneum swelling. Biophysical and computer assisted quantitative assessments, Arch. Dermatol. Res. 289 (1997) 506–513.
[36] D.M. Reilly, D. Ferdinando, C. Johnston, C. Shaw, K.D. Buchanan, M.R. Green, The epidermal nerve fibre network: characterization of nerve fibres in human skin by confocal microscopy and assessment of racial variations, Br. J. Dermatol. 137 (1997) 163–170.
[37] M.K. Hordinsky, M.E. Ericson, Relationship between follicular nerve supply and alopecia, Dermatol. Clin. 14 (1996) 651–660.
[38] M. Hara, M. Toyoda, M. Yaar, J. Bhawan, E.M. Avila, I.R. Penner, B.A. Gilchrest, Innervation of melanocytes in human skin, J. Exp. Med. 184 (1996) 1385–1395.
[39] W.R. Kennedy, G. Wendelschafer-Crabb, T.C. Brelje, Innervation and vasculature of human sweat glands: an immunohistochemistry-laser scanning confocal fluorescence microscopy study, J. Neurosci. 14 (1994) 6825–6833.
[40] D. Guinard, Y. Usson, C. Guillermet, R. Saxod, PS-100 and NF 70-200 double immunolabeling for human digital skin meissner corpuscle 3D imaging, J. Histochem. Cytochem. 48 (2000) 295–302.
[41] D. Guinard, Y. Usson, C. Guillermet, R. Saxod, Merkel complexes of human digital skin: three-dimensional imaging with confocal laser microscopy and double immunofluorescence, J. Comp. Neurol. 398 (1998) 98–104.
[42] D.A. Simone, M. Nolano, T. Johnson, G. Wendelschafer-Crabb, W.R. Kennedy, Intradermal injection of capsaicin in humans produces degeneration and subsequent reinnervation of epidermal nerve fibers: correlation with sensory function, J. Neurosci. 18 (1998) 8947–8959.
[43] X. Navarro, E. Verdu, G. Wendelschafer-Crabb, W.R. Kennedy, Immunohistochemical study of skin reinnervation by regenerative axons, J. Comp. Neurol. 380 (1997) 164–174.
[44] P. Corcuff, C. Bertrand, J.L. Leveque, Morphometry of human epidermis in vivo by real-time confocal microscopy, Arch. Dermatol. Res. 285 (1993) 475–481.
[45] B.R. Masters, P.T. So, Confocal microscopy and multi-photon excitation microscopy of human skin in vivo, Opt. Express 8 (2001) 2–10.
[46] D. Aghassi, R.R. Anderson, S. Gonzalez, Confocal laser microscopic imaging of actinic keratoses in vivo: a preliminary report, J. Am. Acad. Dermatol. 43 (2000) 42–48.
[47] M. Rajadhyaksha, S. Gonzalez, J.M. Zavislan, R.R. Anderson, R.H. Webb, In vivo confocal scanning laser microscopy of human skin II: advances in instrumentation and comparison with histology, J. Invest. Dermatol. 113 (1999) 293–303.
[48] L.C. Swindle, S.G. Thomas, M. Freeman, P.M. Delaney, View of normal human skin in vivo as observed using fluorescent fiber-optic confocal microscopic imaging, J. Invest. Dermatol. 121 (2003) 706–712.
[49] M.B. Delgado-Charro, R.H. Guy, Transdermal iontophoresis for controlled drug delivery and non-invasive monitoring, STP Pharma Sci. 11 (2001) 403–414.
[50] N.G. Turner, R.H. Guy, Iontophoretic transport pathways: dependence on penetrant physicochemical properties, J. Pharm. Sci. 86 (1997) 1385–1389.
[51] P. Greenspan, E.P. Mayer, S.D. Fowler, Nile red: a selective fluorescent stain for intracellular lipid droplets, J. Cell Biol. 100 (1985) 965–973.
[52] M.M. Kneen, D.G. Harkin, L.L. Walker, D. Alcorn, P.J. Harris, Imaging of renal medullary interstitial cells in situ by confocal fluorescence microscopy, Anat. Embryol. 200 (1999) 117–121.
[53] H.J. Bidmon, J.D. Pitts, H.F. Solomon, J.V. Bondi, W.E. Stumpf, Estradiol distribution and penetration in rat skin after topical application, studied by high resolution autoradiography, Histochemistry 95 (1990) 43–54.
[54] N.G. Turner, R.H. Guy, Visualization and quantitation of iontophoretic pathways using confocal microscopy, J. Invest. Dermatol. Symp. Proc. 3 (1998) 136–142.
[55] A. Entwistle, M. Noble, The quantification of fluorescent emission from biological samples using analysis of polarization, J. Microsc. 165 (1992) 347–365.
[56] N.G. Turner, L. Ferry, M. Price, C. Cullander, R.H. Guy, Iontophoresis of poly-L-lysines: the role of molecular weight?, Pharm. Res. 14 (1997) 1322–1331.
[57] P.J. White, A.C. Gray, R.D. Fogarty, R.D. Sinclair, S.P. Thumiger, G.A. Werther, C.J. Wraight, C-5 propyne-modified oligonucleotides penetrate the epidermis in psoriatic and not normal human skin after topical application, J. Invest. Dermatol. 118 (2002) 1003–1007.
[58] V. Regnier, V. Preat, Localization of a FITC-labeled phosphorothioate oligodeoxynucleotide in the skin after topical delivery by iontophoresis and electroporation, Pharm. Res. 15 (1998) 1596–1602.
[59] C. Brus, P. Santi, P. Colombo, T. Kissel, Distribution and quantification of polyethylenimine oligodeoxynucleotide complexes in human skin after iontophoretic delivery using confocal scanning laser microscopy, J. Control. Release 84 (2002) 171–181.
[60] B.S. Grewal, A. Naik, W.J. Irwin, G. Gooris, C.J. de Grauw, H.G. Gerritsen, J.A. Bouwstra, Transdermal macromolecular delivery: real-time visualization of iontophoretic and chemically enhanced transport using two-photon excitation microscopy, Pharm. Res. 17 (2000) 788–795.
[61] M. Kirjavainen, A. Urtti, J. Monkkonen, J. Hirvonen, Influence of lipids on the mannitol flux during transdermal iontophoresis in vitro, Eur. J. Pharm. Sci. 10 (2000) 97–102.
[62] A. Jadoul, H. Tanojo, V. Preat, J.A. Bouwstra, F. Spies, H.E. Boddé, Electroperturbation of human stratum corneum fine structure by high voltage pulses: a freeze-fracture electron microscopy and differential thermal analysis study, J. Invest. Dermatol. Symp. Proc. 3 (1998) 153–158.
[63] M.R. Prausnitz, J.A. Gimm, R.H. Guy, R. Langer, J.C. Weaver, C. Cullander, Imaging regions of transport across human stratum corneum during high-voltage and low-voltage exposures, J. Pharm. Sci. 85 (1996) 1363–1370.
[64] C. Lombry, N. Dujardin, V. Preat, Transdermal delivery of macromolecules using skin electroporation, Pharm. Res. 17 (2000) 32–37.
[65] S. Mitragotri, D.A. Edwards, D. Blankschtein, R. Langer, A mechanistic study of ultrasonically-enhanced transdermal drug delivery, J. Pharm. Sci. 84 (1995) 697–706.

[66] J. Kost, U. Pliquett, S. Mitragotri, A. Yamamoto, R. Langer, J. Weaver, Synergistic effect of electric field and ultrasound on transdermal transport, Pharm. Res. 13 (1996) 633–638.
[67] G. Merino, Y.N. Kalia, M.B. Delgado-Charro, R.O. Potts, R.H. Guy, Frequency and thermal effects on the enhancement of transdermal transport by sonophoresis, J. Control. Release 88 (2003) 85–94.
[68] R. Alvarez-Román, G. Merino, Y.N. Kalia, R.H. Guy, Skin permeability enhancement by low frequency sonophoresis: lipid extraction and transport pathways, J. Pharm. Sci. 92 (2003) 1138–1146.
[69] J.A. Bouwstra, P.L. Honeywell-Nguyen, Skin structure and mode of action of vesicles, Adv. Drug Deliv. Rev. 54 (Suppl 1) (2002) S41–S55.
[70] M.E. Meuwissen, J. Janssen, C. Cullander, H.E. Junginger, J.A. Bouwstra, A cross-section device to improve visualization of fluorescent probe penetration into the skin by confocal laser scanning microscopy, Pharm. Res. 15 (1998) 352–356.
[71] M.E. Kuijk-Meuwissen, H.E. Junginger, J.A. Bouwstra, Interactions between liposomes and human skin in vitro, a confocal laser scanning microscopy study, Biochim. Biophys. Acta 1371 (1998) 31–39.
[72] M.E. Kuijk-Meuwissen, L. Mougin, H.E. Junginger, J.A. Bouwstra, Application of vesicles to rat skin in vivo: a confocal laser scanning microscopy study, J. Control. Release 56 (1998) 189–196.
[73] D.D. Verma, S. Verma, G. Blume, A. Fahr, Liposomes increase skin penetration of entrapped and non-entrapped hydrophilic substances into human skin: a skin penetration and confocal laser scanning microscopy study, Eur. J. Pharm. Biopharm. 55 (2003) 271–277.
[74] S. Zellmer, W. Pfeil, J. Lasch, Interaction of phosphatidylcholine liposomes with the human stratum corneum, Biochim. Biophys. Acta 1237 (1995) 176–182.
[75] M. Kirjavainen, A. Urtti, R. Valjakka-Koskela, J. Kiesvaara, J. Monkkonen, Liposome-skin interactions and their effects on the skin permeation of drugs, Eur. J. Pharm. Sci. 7 (1999) 279–286.
[76] J. du Plessis, C. Ramachandran, N. Weiner, D.G. Muller, The influence of particle size of liposomes on the deposition of drug into skin, Int. J. Pharm. 103 (1994) 277–282.
[77] A. Nagayasu, K. Uchiyama, H. Kiwada, The size of liposomes: a factor which affects their targeting efficiency to tumors and therapeutic activity of liposomal antitumor drugs, Adv. Drug Deliv. Rev. 40 (1999) 75–87.
[78] D.D. Verma, S. Verma, G. Blume, A. Fahr, Particle size of liposomes influences dermal delivery of substances into skin, Int. J. Pharm. 258 (2003) 141–151.
[79] S. Zellmer, D. Reissig, J. Lasch, Reconstructed human skin as model for liposome-skin interaction, J. Control. Release 55 (1998) 271–279.
[80] E. Touitou, B. Godin, N. Dayan, C. Weiss, A. Piliponsky, F. Levi-Schaffer, Intracellular delivery mediated by an ethosomal carrier, Biomaterials 22 (2001) 3053–3059.
[81] E. Touitou, N. Dayan, L. Bergelson, B. Godin, M. Eliaz, Ethosomes—novel vesicular carriers for enhanced delivery: characterization and skin penetration properties, J. Control. Release 65 (2000) 403–418.
[82] N. Dayan, E. Touitou, Carriers for skin delivery of trihexyphenidyl HCl: ethosomes vs. liposomes, Biomaterials 21 (2000) 1879–1885.
[83] G. Cevc, A. Schatzlein, H. Richardsen, Ultradeformable lipid vesicles can penetrate the skin and other semi-permeable barriers unfragmented. Evidence from double label CLSM experiments and direct size measurements, Biochim. Biophys. Acta 1564 (2002) 21–30.
[84] A. Schatzlein, G. Cevc, Non-uniform cellular packing of the stratum corneum and permeability barrier function of intact skin: a high-resolution confocal laser scanning microscopy study using highly deformable vesicles (Transfersomes), Br. J. Dermatol. 138 (1998) 583–592.
[85] A. Zimmer, J. Kreuter, J.R. Robinson, Studies on the transport pathway of PBCA nanoparticles in ocular tissues, J. Microencapsul. 8 (1991) 497–504.
[86] P. Calvo, M.J. Alonso, J.L. Vila-Jato, J.R. Robinson, Improved ocular bioavailability of indomethacin by novel ocular drug carriers, J. Pharm. Pharmacol. 48 (1996) 1147–1152.
[87] R. Ghirardelli, F. Bonasoro, C. Porta, D. Cremaschi, Identification of particular epithelial areas and cells that transport polypeptide-coated nanoparticles in the nasal respiratory mucosa of the rabbit, Biochim. Biophys. Acta 1416 (1999) 39–47.
[88] A. Lamprecht, U. Schafer, C.M. Lehr, Size-dependent bioadhesion of micro- and nanoparticulate carriers to the inflamed colonic mucosa, Pharm. Res. 18 (2001) 788–793.
[89] R. Alvarez-Román, A. Naik, Y.N. Kalia, H. Fessi, R.H. Guy, Enhanced dermal delivery from poly(ε-caprolactone) nanospheres: an evaluation by confocal laser scanning microscopy, AAPS, 2002.
[90] R. Alvarez-Román, A. Naik, Y.N. Kalia, R.H. Guy, H. Fessi, Enhancement to topical delivery from biodegradable nanoparticle, Pharm. Res. (2004) (in press).
[91] R. Alvarez-Román, A. Naik, Y.N. Kalia, R.H. Guy, H. Fessi, Skin penetration and distribution of fluorescent nanoparticles, J. Control. Release (2004) (in press).
[92] J. Saunders, H. Davis, L. Coetzee, S. Botha, A. Kruger, A. Grobler, A novel skin penetration enhancer: evaluation by membrane diffusion and confocal microscopy, J. Pharm. Pharm. Sci. 2 (1999) 99–107.
[93] L.A. Pechtold, W. Abraham, R.O. Potts, Characterization of the stratum corneum lipid matrix using fluorescence spectroscopy, J. Invest. Dermatol. Symp. Proc. 3 (1998) 105–109.
[94] P. Uster, P.K. Working, J. Vaage, Pegylated liposomal doxorubicin (DOXIL, CAELYX) distribution in tumour observed with confocal laser scanning microscopy, Int. J. Pharm. 162 (1998) 77–86.
[95] S.M. Niemiec, J.M. Latta, C. Ramachandran, N.D. Weiner, B.J. Roessler, Perifollicular transgenic expression of human interleukin-1 receptor antagonist protein following topical application of novel liposome-plasmid DNA formulations in vivo, J. Pharm. Sci. 86 (1997) 701–708.
[96] P.J. White, R.D. Fogarty, I.J. Liepe, P.M. Delaney, G.A. Werther, C.J. Wraight, Live confocal microscopy of oligonucleotide uptake by keratinocytes in human skin grafts on nude mice, J. Invest. Dermatol. 112 (1999) 887–892.
[97] J. Lasch, R. Laub, W. Wohlrab, How deep intact liposomes penetrate into human skin?, J. Control. Release 18 (1991) 55–58.
[98] P.M. Elias, C. Cullander, T. Mauro, U. Rassner, L. Komuves, B.E. Brown, G.K. Menon, The secretory granular cell: the outermost granular cell as a specialized secretory cell, J. Invest. Dermatol. Symp. Proc. 3 (1998) 87–100.
[99] P. Talreja, N.K. Kleene, W.L. Pickens, T.F. Wang, G.B. Kasting, Visualization of the lipid barrier and measurement of lipid pathlength in human stratum corneum, AAPS Pharm. Sci. 3 (2001) E13.
[100] T. Chen, R. Langer, J.C. Weaver, Charged microbeads are not transported across the human stratum corneum in vitro by short high-voltage pulses, Bioelectrochem. Bioenerg. 48 (1999) 181–192.
[101] A. Rolland, N. Wagner, A. Chatelus, B. Shroot, H. Schaefer, Site-specific drug delivery to pilosebaceous structures using polymeric microspheres, Pharm. Res. 10 (1993) 1738–1744.
[102] N. Katahira, T. Murakami, S. Kugai, N. Yata, M. Takano, Enhancement of topical delivery of a lipophilic drug from charged multilamellar liposomes, J. Drug Target. 6 (1999) 405–414.
[103] A.M. Torche, P. Le Corre, E. Albina, A. Jestin, R. Le Verge, PLGA microspheres phagocytosis by pig alveolar macrophages: influence of poly(vinyl alcohol) concentration, nature of loaded-protein and copolymer nature, J. Drug Target. 7 (2000) 343–354.
[104] N.G. Turner, C. Cullander, R.H. Guy, Determination of the pH gradient across the stratum corneum, J. Invest. Dermatol. Symp. Proc. 3 (1998) 110–113.